

A new dataset of river flood hazard maps for Europe and the Mediterranean Basin region

Francesco Dottori¹, Lorenzo Alfieri², Alessandra Bianchi³, Jon Skoien¹, Peter Salamon¹

1: European Commission, Joint Research Centre, Via E. Fermi 2749, 21027 Ispra, Italy.

2: CIMA Research Foundation, Savona, Italy

3: FINCONS SPA, Italy

Correspondence to: francesco.dottori@ec.europa.eu

Keywords: river flooding, flood hazard mapping, Europe, EFAS, Mediterranean Basin region.

Abstract

Continental scale hazard maps for riverine floods have grown in importance in the last years. Nowadays, they are used for a variety of research and commercial activities, such as evaluating present and future risk scenarios and adaptation strategies, as well as a support of national and local flood risk management plans. Here, we present a new set of high resolution (100m) hazard maps for river flooding that covers most of the geographical Europe and all the river basins entering the Mediterranean and Black Seas in the Caucasus, Middle East and Northern Africa countries. Maps represent inundation along 329'000 km of river network for six different flood return periods, expanding the previous datasets available in the region. The input river flow data is produced by the hydrological model LISFLOOD using new calibration and meteorological data, while inundation simulations are performed with the hydrodynamic model LISFLOOD-FP. In addition, we present a detailed validation exercise using official hazard maps for Hungary, Italy, Norway, Spain and the United Kingdom, that provides a more detailed evaluation of the new dataset in respect to previous works in the region. We find that modelled maps can identify on average two-thirds of reference flood extent, however they also overestimate flood-prone areas for flood probabilities below 1-in-100-year, while for return periods equal or above 500 years the maps can correctly identify more than half of flooded

29 areas. Further verification in North African and Eastern Mediterranean regions is needed to
30 better understand the performance of the flood maps in arid areas outside Europe. We attribute
31 the observed skill to a number of shortcomings of the modelling framework, such as the absence
32 of flood protections and rivers with upstream area below 500 km², and the limitations in
33 representing river channels and topography of low land areas. In addition, the different design
34 of reference maps (e.g. extent of areas included) -affects the correct identification of the areas
35 for the validation, thus penalizing scores. However, modelled maps achieve comparable results
36 to existing large-scale flood models when using similar parameters for the validation. We
37 conclude that recently released high-resolution elevation datasets combined with reliable data of
38 river channel geometry may greatly contribute to improve future versions of continental-scale
39 flood hazard maps. The database is available for download at
40 <http://data.europa.eu/89h/1d128b6c-a4ee-4858-9e34-6210707f3c81> (Dottori et al., 2020a).
41

42 *1) Introduction*

43 Nowadays, flood hazard maps are a basic component of any flood risk management strategy
44 (EC 2007). They provide spatial information about a number of variables (such as flood extent,
45 water depth, flow velocity) that are crucial to quantify flood impacts and therefore to evaluate
46 flood risk. Moreover, they can be used as a powerful communication tool, allowing to quickly
47 visualize the potential spatial impact of a river flood over an area.

48 Continental-scale and global-scale flood maps have grown in importance in the last years, and
49 they are now used for a variety of research, humanitarian and commercial activities, and as a
50 support of national and local flood management (Ward et al., 2015; Trigg et al., 2016). Global
51 flood maps are used to provide flood risk information and support decision-making in spatial
52 and infrastructure planning in countries where national level assessments are not available
53 (Ward et al., 2015). Moreover, continental and global maps are vital for consistent
54 quantification of flood risk and in projecting the impacts of climate change (Alfieri et al., 2015;
55 Trigg et al., 2016; Dottori et al., 2018), allowing for comparisons between different regions,
56 countries and river basins (Alfieri et al., 2016). Quantitative and comparable flood risk
57 assessments are also necessary to derive measurable indicators of the targets set by international
58 agreements such as the Sendai Framework for Disaster Risk Reduction (UNISDR, 2015).

59 In Europe, continental-scale flood hazard maps have been produced by Barredo et al. (2007),
60 Feyen et al. (2012), Alfieri et al. (2014), [Dottori et al. \(2016a\)](#) and Paprotny et al. (2017). These
61 maps have been used for a variety of studies, such as the evaluation of river flood risk under
62 future socio-economic and climate scenarios (Barredo et al., 2007; Feyen et al., 2012; Alfieri et
63 al., 2015), the evaluation of flood adaptation measures (Alfieri et al., 2016) and near-real time
64 rapid risk assessment (Dottori et al., 2017).

65 The quality of continental-scale flood maps is constantly improving thanks to the increasing
66 accuracy of datasets and modelling tools. Wing et al., (2017) developed a dataset of flood
67 hazard maps for the conterminous United States using detailed national datasets and high-
68 resolution hydrodynamic modelling, and demonstrated that continental-scale maps can achieve
69 an accuracy similar to official national hazard maps, including maps based on accurate local-
70 scale studies. Moreover, Wing et al. used the same official hazard maps to evaluate the
71 performance of the global flood hazard model developed by Sampson et al. (2015). While the
72 global model was less accurate than continental model, it could correctly identify over two-

73 thirds of flood extent. Conversely, European-scale maps have undergone limited testing against
74 official hazard maps, due to limitations in accessing official data (Alfieri et al., 2014).

75 Here, we present a new set of flood hazard maps at 100m resolution (Dottori et al., 2020a),
76 developed as a component of the Copernicus European Flood Awareness System (EFAS,
77 www.efas.eu). The new dataset builds upon the map catalogue developed by Dottori et al
78 (2016a) and feature different advances. The geographical extent of the new maps has been
79 expanded to include all geographical Europe (with the exclusion of the Volga river basin), the
80 rivers entering the Mediterranean Sea and the Black Sea (with the partial inclusion of the Nile
81 river basin), plus Turkey, Syria and the Caucasus region. To our best knowledge these are the
82 first flood hazard maps available at 100m resolution for the whole Mediterranean Basin region.
83 The hydrological input is calculated using the latest version of the LISFLOOD hydrological
84 model (van der Knijff et al., 2010; Burek et al, 2013; <https://ec-jrc.github.io/lisflood/>), based on
85 updated calibration and meteorological data in respect to the previous dataset by Dottori et al.
86 (2016a). Flood simulations are performed with the hydrodynamic model LISFLOOD-FP (Bates
87 et al., 2010; Shaw et al., 2021), following the approach developed by Alfieri et al., (2014;
88 2015).

89 To provide a comprehensive overview of the skill of the new maps, we perform a validation
90 exercise using official hazard maps for a number of countries, regions and large river basins in
91 Europe. The number and extent of the validation sites allows for a more detailed evaluation in
92 respect to previous efforts by Alfieri et al. (2014) and Paprotny et al. (2017), even though none
93 of the validation sites is located outside Europe due the unavailability of national flood maps.
94 Moreover, we discuss the results of the validation in light of previous literature studies, we
95 compare the performance of the present and previous version of the flood map dataset, and we
96 discuss a number of tests with alternative datasets and methods.

97 *2) Data and methods*

98 In this Section we describe the procedure adopted to produce and validate the flood hazard
99 maps. The hydrological input consists of daily river flow for the years 1990-2016. It was
100 produced with the latest version of the hydrological model LISFLOOD (Section 2.1), based on
101 interpolated daily meteorological observations. River flow data are analysed to derive frequency
102 distributions, peak discharges and flood hydrographs, as described in Section 2.2. Flood

103 hydrographs are then used to simulate flooding processes at local scale with the LISFLOOD-FP
104 hydrodynamic model (Section 2.3). Finally, Section 2.4 describes the validation exercise and
105 the comparison of different approaches and input datasets.

106 *2.1 The LISFLOOD model*

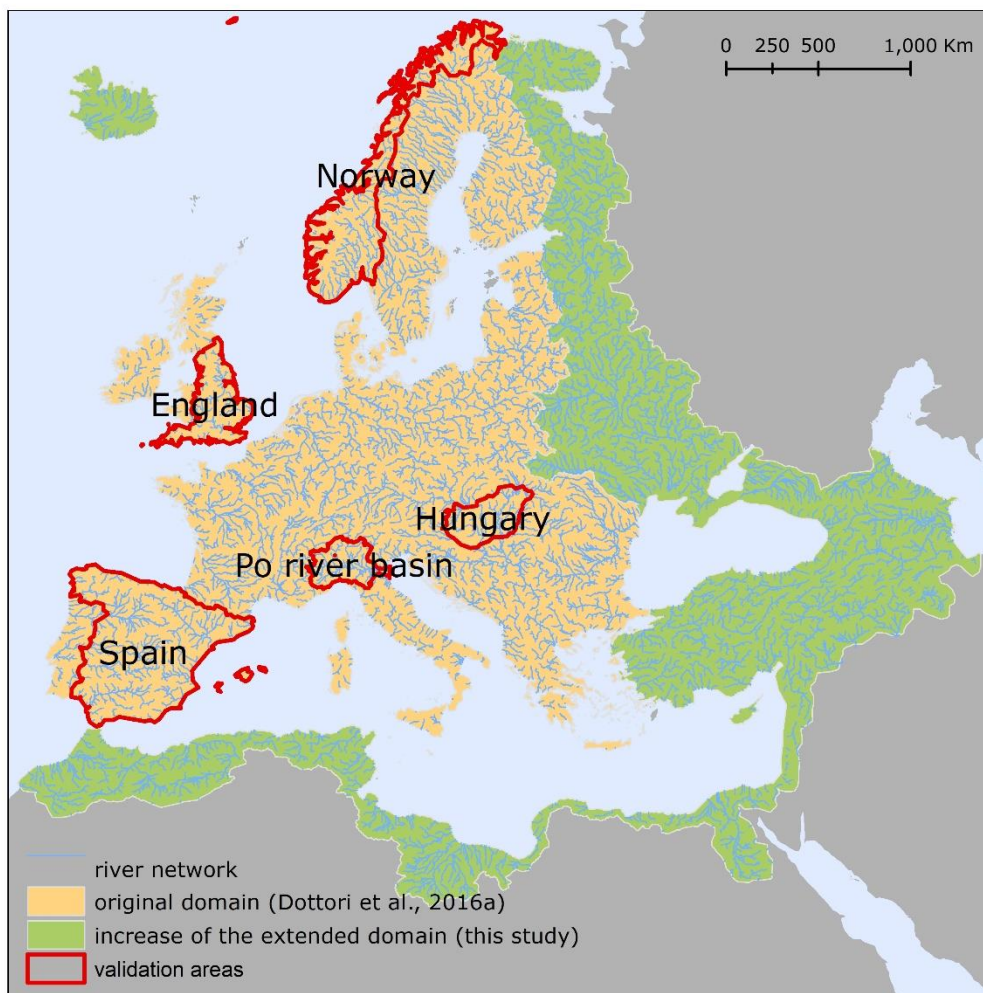
107 LISFLOOD (Burek et al, 2013; van der Knijff et al., 2010) is a distributed, physically-based
108 rainfall-runoff model combined with a routing module for river channels. In this work we use
109 the latest updated version of LISFLOOD, released as open-source software and available at
110 <https://ec-jrc.github.io/lisflood/>. The model is applied to run a long-term hydrological
111 simulation for the period 1990-2016 at 5 km grid spacing and daily resolution, which provides
112 the hydrological input for the flood simulations. Note that the same simulation also provides
113 initial conditions for daily flood forecast issued by EFAS.

114 The long-term run of LISFLOOD is driven by gridded meteorological maps, derived by
115 interpolating meteorological observations from stations and precipitation datasets (see
116 Appendix A for details). The meteorological dataset has been updated in respect to the dataset
117 used by Dottori et al. (2016a) to include new stations and gridded datasets across the new EFAS
118 domain (Arnal et al. 2019). In addition, LISFLOOD simulations require a number of static input
119 maps such as land cover, digital elevation model, drainage network, soil parameters and
120 parameterization of reservoirs. All the static maps have been updated to cover the whole EFAS
121 domain depicted in Figure 1.

122 The current LISFLOOD version also benefits from an updated calibration at European scale,
123 based on the Evolutionary Algorithm approach (Hirpa et al., 2018) with the modified Kling-
124 Gupta efficiency criteria (KGE; Gupta et al., 2009) as objective function, and streamflow data
125 for 1990-2016 from more than 700 gauge stations. The results of the calibration and the
126 LISFLOOD hydrological skill are described in Arnal et al (2019), and summarized in the
127 Appendix B. We did not carry out a formal comparison with the previous LISFLOOD
128 calibration, which used a different algorithm and performance indicators (Zajac et al., 2013),
129 however the larger dataset of streamflow observations and the improvement of the calibration
130 routines should provide a better performance.

131 The geographical extent used in the present study to produce the flood maps follows the recent
132 enlargement of EFAS (Arnal et al., 2019), and it is shown in Figure 1. The new domain is

133 approximately 8'930'000 km² wide (an increase of 76% in respect with the previous extent). It
134 covers the entire geographical Europe (with the exclusion of the Volga river basin and a number
135 of river basins of the Arctic Sea in Russia), all the rivers entering the Mediterranean and Black
136 Seas (with a partial inclusion of the Nile river basin), plus the entire territories of Armenia,
137 Georgia, Turkey, and most of Syria and Azerbaijan. The river network included in the new
138 flood hazard maps has a total length of 329'000 km, with an 80% increase compared to the
139 previous flood maps (Alfieri et al., 2015; Dottori et al., 2016a).



140
141 *Figure 1. Geographical extent of the EFAS extended domain covered by the present dataset of*
142 *flood hazard maps. The extent of the map dataset produced by Dottori et al. (2016a) is depicted*
143 *in beige, while the regions added with the extended domain are in green. The figure also*
144 *displays the river network considered by the flood maps and the areas used for the validation*
145 *exercise (see Sections 2.3 and 3).*

2.2 Hydrological input of flood simulations

The input hydrographs necessary for the flood simulations are derived from the LISFLOOD streamflow dataset described in Section 2.1, following the approach proposed by Alfieri et al. (2014). Streamflow data is available for the EFAS river network at 5 km grid spacing for rivers with upstream drainage areas larger than 500 km². For each pixel of the river network we selected annual maxima over the period 1990-2016 and we used the L-moments approach to fit a Gumbel distribution and calculate peak flow values for reference return periods of 10, 20, 50, 100, 200 and 500 years. Note that we also calculated the 30- and 1000-year return periods in limited parts of the model domain to allow validation against official hazard maps, see Section 2.3.

Subsequently, we calculate a Flow Duration Curve (FDC) from the long-term simulation. The FDC is obtained by sorting in decreasing order all the daily discharges, thus providing annual maximum values Q_D for any duration i between 1 and 365 days. Annual maximum values are then averaged over the entire period of data, and used to calculate the ratios ε_i between each average maximum discharge for i -th duration $Q_{D(i)}$ and the average annual peak flow (i.e. $Q_D = 1$ day). Design flood hydrographs are derived using daily time steps. The peak value is given by the peak discharge for the selected T - year return period Q_T , while the other values Q_i are derived multiplying Q_T by the ratio ε_i . The hydrograph peak Q_T is placed in the centre of the hydrograph, while the other values Q_i are sorted alternatively to produce a triangular hydrograph shape, as shown in Figure 2.

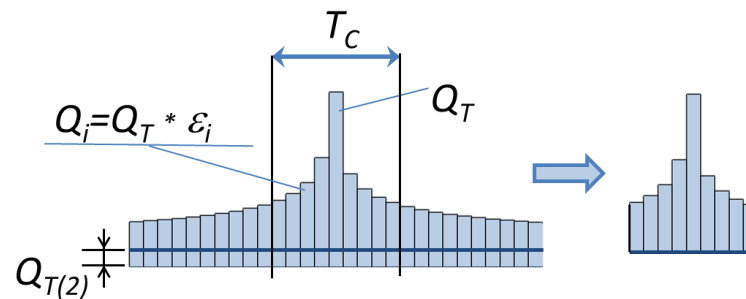


Figure 2. General scheme of flood hydrographs (adapted from Alfieri et al., 2014).

Because river channels are usually not represented in continental scale topography, flood hydrograph values are reduced by subtracting the 2-years discharge peak $Q_{T(2)}$, which is

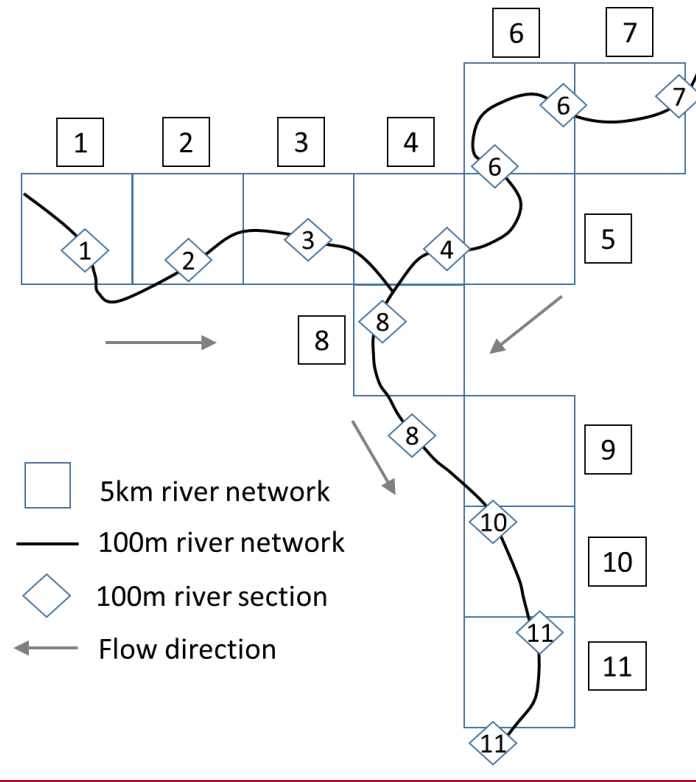
171 commonly considered representative of river bank-full conditions. Note that the original DEM
172 is not modified. The total duration of the hydrograph is given by the local value of the time of
173 concentration T_c , therefore all the durations $> T_c$ are discarded from the final hydrograph.
174

175 *2.3 Flood hazard mapping*

176 The continental-scale flood hazard maps are derived from local flood simulations run all along
177 the river network as in Alfieri et al. (2014). We use the DEM at 100 m resolution developed for
178 the Catchment Characterization and Modelling Database (CCM; Vogt et al., 2007) to derive a
179 high-resolution river network at the same resolution. Along this river network we identify
180 reference sections every 5 km along stream-wise direction, and we link each section to the
181 closest upstream section (pixel) of the EFAS 5km river network, using an partially automated
182 procedure to ensure a correct linkage near confluences. In this way, the hydrological variables
183 necessary to build the flood hydrographs can be transferred from the 5km to the 100m river
184 network. Figure 3 describes how the 5km and 100m river sections are linked using a conceptual
185 scheme.

186 Then, for every 100 m river section we run flood simulations using the 2D hydrodynamic model
187 LISFLOOD-FP (Shaw et al., 2021), to produce a local flood map for each of the six reference
188 return periods. Simulations are based on the local inertia solver of LISFLOOD-FP developed by
189 Bates et al. (2010), which is now available as open-source software
190 (<https://www.seamlesswave.com/LISFLOOD8.0>). We use the CCM DEM as elevation data, the
191 synthetic hydrographs described in Section 2.2 as hydrological input, and a mosaic of Corine
192 Land Cover for the year 2016 (Copernicus LMS, 2017) and GlobCover for the year 2009
193 (Bontemps et al., 2009) to estimate the friction coefficient based on land use.

194 Finally, the flood maps with the same return period are merged together to obtain the
195 continental-scale flood hazard maps. The 100m river network is included as a separate map in
196 the dataset, to delineate which water courses have been considered in the creation of the flood
197 hazard maps.



198

199 *Figure 3. Conceptual scheme of the EFAS river network (5 km, squares) with the high-*
 200 *resolution network (100 m) and river sections (diamonds) where flood simulations are derived.*
 201 *The related sections of the two networks are indicated by the same number. Source: Dottori et*
 202 *al. (2017).*

203

204 It is important to note that the flood maps developed do not take into account the influence of
 205 local flood defences, in particular dyke systems. Such limitation has been dictated mainly by the
 206 absence of consistent data at European scale. None of the available DEMs for Europe have the
 207 necessary accuracy and resolution to embed artificial embankments into elevation data.
 208 Moreover, there are no publicly available continental or national datasets describing the location
 209 and characteristics (e.g. dyke height, distance from river channel) of flood protections.
 210 Currently available datasets are based on the design return period of flood protection, e.g. the
 211 maximum return period of flood events that protections can withstand before being overflowed,
 212 (Jongman et al., 2014; Scussolini et al., 2016). Most of the protection standards reported by
 213 these datasets for Europe are based on empirical regressions derived using proxy variables (e.g.
 214 gross domestic product, land use), with few data based on actual design standards. While these
 215 datasets have been applied to calculate flood risk scenarios (Alfieri et al., 2015) and flood

216 impacts (Dottori et al., 2017), they have important limitations when used for mapping flood
217 extent. Wing et al. (2017) linked the flood return period of protection standards with flood
218 frequency analysis to adjust the bank height of the river channels, however with impaired
219 performance of the model. Moreover, recent studies for United States suggest that empirical
220 regressions based on gross domestic product and land use may not be reliable (Wing et al.,
221 2019).

222 Despite these limitations, maps not accounting for physical flood defences may be applied to
223 estimate the flood hazard in case of failure of the protection structures, and for flood events
224 exceeding protections levels.

225 *2.3 Validation of flood hazard maps*

226 *2.3.1 Selection of validation areas and maps*

227 The validation of large-scale flood hazard maps requires the use of benchmarks with one or
228 more datasets with extension and accuracy commensurate to the modelled maps. For instance
229 Wing et al. (2017) used the official hazard maps developed for the conterminous United States
230 to evaluate the performance of two flood hazard models, respectively designed to produce
231 global-scale and continental-scale flood maps (see Introduction). In Europe, all member states
232 of the European Union as well as the United Kingdom have developed national datasets of
233 flood hazard maps for a range of flood probabilities (usually expressed with the flood return
234 period), following the guidelines of the EU Floods Directive (EC 2007). While these maps are
235 generally available online for consultation on Web-GIS services, only few countries and river
236 basin authorities make the maps available for download in a format that allows comparison with
237 geospatial data. Table 1 presents the list of flood hazard maps that could be retrieved and used
238 for the validation exercise, while Figure 1 shows their geographical distribution. Note that the
239 relevant links to access these maps are provided in the Data Availability section.

240 Even though more official maps are likely to become available in the near future, the maps here
241 considered offer an acceptable overview of the different climatic zones and floodplain
242 characteristics of the European continent. Conversely, we could not retrieve national or regional
243 flood hazard maps outside Europe, meaning the skill of the modelled maps could not be tested
244 in the arid regions in Northern Africa and Eastern Mediterranean. In Norway, Spain, the United

245 Kingdom and the Po River Basin the official maps take into account flood defences, which are
 246 instead not represented in the modelling framework. Official maps for England also include
 247 areas prone to coastal flooding events (such as tidal and storm surges). None of the official
 248 maps include areas prone to pluvial flooding, which are therefore not considered in this
 249 analysis.

250 For the comparison exercise, we selected available maps for return periods for which flood
 251 extent is likely to be less conditioned by flood defences. For instance, the main stem of the Po
 252 river is protected against the 1-in-200-year flood events (Wing et al., 2019), whereas protection
 253 standards in England and Norway are usually above 20 years (Scussolini et al., 2016).
 254 Conversely, we consider the 1-in-30-year map for Hungary and the 1-in-10-year map for Spain
 255 because flood defences are either not accounted for (Hungary) or their extent and design level is
 256 not known (Spain).

257

Country	Geographical extent	Return periods used	Defences included
Hungary	Country scale	30 – 100 - 1000 years	No
Italy	Po River Basin	500 years	Yes
Norway	Country scale	100 years	Yes
Spain	Country scale	10 -100 - 500 years	Yes
United Kingdom	England	100 - 1000 years	Yes

258 *Table 1. List and characteristics of the flood hazard maps used in the validation exercise.* The
 259 links for downloading the maps are provided in the Data Availability section.

260 2.3.2 Performance metrics and validation procedure

261 The national flood hazard maps listed in Table 1 are provided as polygons of flood extent, with
 262 no information on water depth nor on original resolution of data. According to Sampson et al.
 263 (2015), the official flood hazard maps for England are constructed using DEMs of at least 5 m

264 resolution, therefore flood extent maps should be of comparable resolution. Reference flood
 265 maps for the Po basin and Spain are likely to have a similar resolution since they are based on
 266 LIDAR elevation data (MITECO 2011). For the comparison, official reference maps have been
 267 converted to raster format with the same resolution as the modelled maps (i.e. 100m), while the
 268 latter have been converted to binary flood extent maps. To improve the comparison between
 269 modelled and reference maps we applied a number of corrections. First, we used the CORINE
 270 Land Cover map to exclude permanent water bodies (river beds of large rivers or estuaries,
 271 lakes, reservoirs, coastal lagoons) from the comparison. Second, we restricted the comparison
 272 area around modelled maps to exclude the elements of river network (e.g. minor tributaries)
 273 included in the reference maps but not in the modelled maps. We used a different buffer extent
 274 according to each study area, considering the floodplain morphology and the variable extent and
 275 density of mapped river network. For instance, in Hungary we applied a 10-km buffer around
 276 modelled maps to include the large flooded areas reported in reference maps and avoid
 277 overfitting. In England, we used a 5-km buffer due to the high density of the river network
 278 mapped in the official maps; the buffer is also applied to mask out coastal areas far from rivers
 279 estuaries, because official maps include flood-prone areas due to 1-in-200-year coastal flood
 280 events. We calculated that flood-prone areas inside the 5km buffer correspond to 73% of the
 281 total extent for the 1-in-100-year flood. For the Po river Basin, we excluded from the
 282 comparison the areas belonging to the Adige River Basin and the lowland drainage network,
 283 which are not included in the official hazard maps. In Spain and Norway official flood hazard
 284 maps have only been produced where relevant assets are at risk, according to available
 285 documentation [MITECO 2011; NVE 2020]. We therefore restricted the comparison only to
 286 areas where official flood hazard maps have been produced. Table 2 provide the list of
 287 parameters used to determine the areas used for the comparison.

Test area	Buffer value (reference maps)	Buffer value (modelled maps)
Hungary	NA	10 km
Po River Basin	NA	See main text
Norway	5 km	5 km

Spain	5 km	5 km
England	NA	5 km

288 *Table 2. List of parameters used to determine the extent of areas used for comparing reference*
289 *and modelled maps (NA: buffer not applied).*

290
291 We evaluate the performance of simulated flood maps against reference maps using a number of
292 indices proposed in literature (Bates and De Roo, 2000; Alfieri et al., 2014; Dottori et al.,
293 2016b; Wing et al., 2017). The hit ratio HR evaluates the agreement of simulated maps with
294 observations and it is defined as:

$$295 \quad HR = (Fm \cap Fo) / (Fo) \times 100 \quad (1)$$

296 where $Fm \cap Fo$ is the area correctly predicted as flooded by the model, and Fo indicates the
297 total observed flooded area. HR scores range from 0 to 1, with a score of 1 indicating that all
298 wet cells in the benchmark data are wet in the model data. The formulation of the hit ratio does
299 not penalize overprediction, which can be instead quantified using the false alarm ratio FAR:

$$300 \quad FAR = (Fm / Fo) / (Fm) \times 100 \quad (2)$$

301 where Fm / Fo is the area wrongly predicted as flooded by the model. FAR scores range from 0
302 (no false alarms) to 1 (all false alarms). Finally, a more comprehensive measure of the
303 agreement between simulations and observations is given by the critical success index CSI,
304 defined as:

$$305 \quad CSI = (Fm \cap Fo) / (Fm \cup Fo) \times 100 \quad (3)$$

306 where $Fm \cup Fo$ is the union of observed and simulated flooded areas. - CSI scores range from 0
307 (no match between model and benchmark) to 1 (perfect match between benchmark and model).

308 **2.4 Additional tests**

309 To choose the best possible methodologies and datasets to construct the flood hazard maps, we
310 have performed a number of tests using recent input datasets as well as by alternative strategies
311 to account for vegetation effects on elevation data.

312

313

314 *2.4.1 Elevation data*

315 It is well recognized that the quality of flood hazard maps strongly depend on the accuracy of
316 elevation data used for modelling (Yamazaki et al., 2017). This is especially crucial for
317 continental scale maps, since the quality of available elevation datasets is rarely commensurate
318 to the accuracy required for modelling flood processes [Wing et al., 2017]. Moreover, high-
319 resolution and accurate elevation data such as LIDAR-based DEMs cannot be used for reasons
320 of consistency, given that these data are only available for few areas and countries.

321 The recent release of new global elevation models have the potential for improving the accuracy
322 of large scale flood simulations, and hence the quality of flood hazard maps. Here, we test the
323 use of the MERIT DEM (Yamazaki et al., 2017) within the proposed modelling approach and
324 we compare the results with those obtained with CCM DEM. The MERIT DEM is based on the
325 SRTM data, similarly to CCM DEM, however it has been extensively corrected and improved
326 through comparisons from other large scale datasets, to eliminate error biases, to improve data
327 accuracy at high latitudes (areas above 60° are not covered by SRTM) and compensate for
328 factors like vegetation cover. Note that areas above 60° in CCM DEM were derived from
329 national datasets, and therefore it is where the two datasets are likely to differ most.

330 *2.4.2 Correction of elevation data with land use*

331 The CCM DEM elevation dataset is mostly based on SRTM data and therefore elevation data
332 can be spuriously increased by the effect of vegetation canopy in densely vegetated areas, and
333 by buildings in urban areas. Recent research works proposed advanced techniques to remove
334 surface artefacts, based on artificial neural networks (Wendi et al., 2016, Kulp and Strauss,
335 2018) or other machine learning methods (Liu et al., 2018; Meadows and Wilson, 2021). Most
336 approaches correct DEM elevation with higher-accuracy datasets, using auxiliary data such as
337 tree density and height for correcting vegetation bias (as done for the MERIT-DEM by
338 Yamazaki et al., 2017), whereas elevation bias in urban areas can be corrected using night light,
339 population density, or Open Street Map elevation data (Liu et al., 2018). Given that improving
340 elevation data is not the main scope of this work, we opted for applying a simpler method for
341 quickly correcting the CCM DEM elevation data. Specifically, we use the land cover map
342 derived from Corine Land Cover and GlobCover to identify densely vegetated areas and urban
343 areas, and we applied a correction factor as a function of local land use to locally reduce

344 elevation. The correction factor varies from 8m for dense forested areas, to 2m for urban areas.
345 Note that this values are based on the findings of previous literature studies such as Baugh et al.
346 (2013) and Dottori et al. (2016b), while a formal calibration was not undertaken.

347 *3) Results and discussion*

348 We present the outcomes of the validation exercise by describing first the general results at
349 country and regional scale in Section 3.1. Then, we discuss in the main text the outcomes for
350 England, Hungary and Spain (Section 3.2), while the Norway and Po river basin case studies are
351 presented in the Appendix C. We also complement the analysis with additional validation over
352 major river basins in England and Spain. In Section 3.3 we compare our results with the
353 validation exercise carried out by Wing et al. (2017) and with the findings of other literature
354 studies. Finally, in Section 3.4 and 3.5 and Appendix B we compare the performance of the
355 present and previous version of the flood map dataset, and we discuss the results of the tests
356 with different elevation data and strategies to account for vegetation.

357 *3.1 Validation of modelled maps at national and regional scale*

358 Table 3 presents the results of the validation for each testing area and return period. The
359 performance metrics are calculated using the total extent of the reference and modelled maps
360 with the same return period. The first visible outcome is the low scores for the comparisons
361 with reference maps with high probability of flooding, i.e. low flood return periods (<30 years).
362 Performances improve markedly with the increasing of return periods; due to the decrease of
363 false alarm rate FAR, while the hit rate HR does not vary significantly. In particular, critical
364 success index (CSI) values approach 0.5 for the low probability flood maps, i.e., for return
365 periods equal or above 500 years. Considering that most of the reference flood maps include the
366 effect of flood defences (contrary to the modelled maps), these results suggest that the majority
367 of rivers in the study areas may be protected for flood return periods around 100 years or lower,
368 as indeed reported by available flood defence databases (Scussolini et al., 2016). Differences
369 between simulated and reference hydrological input are likely to influence the skill of modelled
370 flood maps. However, further analyses are difficult because we have no specific information on
371 the hydrological input used for the reference flood maps (e.g. peak flows, hydrograph shape). In
372 the following sections, we use the skill of the LISFLOOD long-term simulation to evaluate the

373 agreement between modelled and observed hydrological regime, but this does not necessarily
 374 translate to extreme values. High-probability floods are also sensitive to the method used to
 375 reproduce river channels, and the simplified approach used in this study might underestimate
 376 the conveyance capacity of channels (see Section 3.2.2 for an example). Finally, the better
 377 performance for low-probability floods may also depend on floodplain morphology, where
 378 valley sides create a morphological limit to flood extent.

	RP	HR	FAR	CSI
Spain	10	0.58	0.65	0.28
Hungary	30	0.77	0.88	0.11
Spain	100	0.63	0.44	0.42
Hungary	100	0.76	0.74	0.24
Norway	100	0.70	0.72	0.25
England	100	0.53	0.31	0.43
Po River Basin	500	0.60	0.13	0.56
Spain	500	0.61	0.36	0.45
Hungary	1000	0.76	0.45	0.47
England	1000	0.52	0.12	0.48

379 *Table 3. Results of the validation against official flood hazard maps: value of the performance*
 380 *indices at country and regional scale. RP=Return Period, HR=Hit Ratio, FAR= False Alarm*
 381 *Ratio, CSI=Critical Success Index.*

382

383 **3.2 Discussion of modelled maps results at national and regional scale**

384 The results in Table 3 highlight considerable differences in the skill of the flood maps across
 385 countries and regions. While some differences may arise from the variability of floodplain
 386 morphology and model input data, others are attributable to the different methods applied to
 387 produce the reference maps (MITECO 2011; NVE 2020). In the following sections we examine
 388 in more detail the outcomes for each study area.

389

390

391 **3.2.1 England**

392 According to Table 3, modelled flood maps tend to underestimate flood extent in England, as
 393 visible by the hit rate values around 0.5 (e.g. out of every two flooded cells, only one is
 394 correctly identified as flooded by the model). Such result is confirmed when focusing the
 395 analysis on the major river basins of England, as reported in Table 4. Notably, ~~hit rates~~HR has
 396 generally marginal or no increases with the increase of return period considered, while FAR
 397 values have a marked decrease. The results of reported by Arnal et al. (2019) and summarized
 398 in Figure B1 suggest a fair hydrological skill of the LISFLOOD calibration in England, with
 399 KGE values generally above 0.5. However, there is not a clear correlation between hydrological
 400 and flood map skill, with some basins (e.g. Thames) showing high KGE values but relatively
 401 low CSI values.

402 For the Thames basin, the low CSI value is likely influenced by the tidal flooding component
 403 from London eastwards. According to Sampson et al. (2015), the official flood hazard map
 404 assumes a 1 in 200 year coastal flood along with failure of the Thames tidal barrier, whereas our
 405 river flood simulations use the mean sea level as boundary condition and do include storm surge
 406 and tidal flooding. Concurrent fluvial-tidal flooding processes occur in other river estuaries, so
 407 this might reduce the skill of the modelled maps. Furthermore, the Thames catchment is heavily
 408 urbanized and has extensive flood defense and alleviation schemes compared the other
 409 catchments (Sampson et al., 2015). Both aspects might increase the elevation bias of CCM
 410 DEM and complicate the correct simulation of extreme flood events.

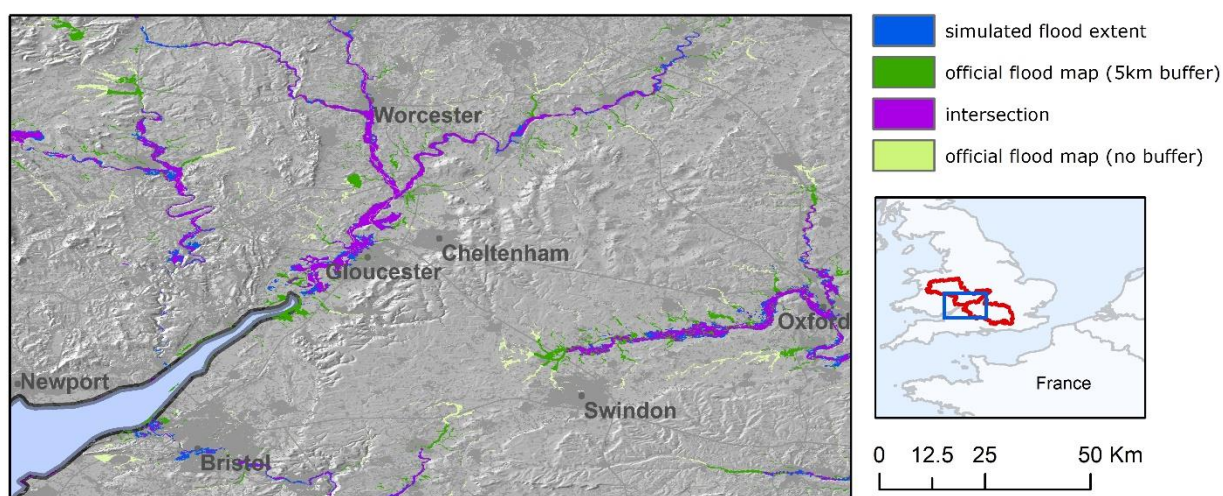
411

Catchments	100-year RP			1000-year RP		
	HR	FAR	CSI	HR	FAR	CSI
England	0.53	0.31	0.43	0.52	0.12	0.48
Ouse	0.57	0.39	0.42	0.56	0.19	0.49
Severn	0.64	0.24	0.53	0.63	0.20	0.54
Thames, above Lea	0.56	0.46	0.38	0.55	0.23	0.47
Trent	0.63	0.28	0.50	0.59	0.06	0.57
Tyne	0.51	0.43	0.37	0.52	0.28	0.43

412 *Table 4. Validation indices in England and in major river basins.*

413

414 Besides these results, the visual inspection of reference maps suggest that the underestimation is
415 mostly partly caused by the high density of mapped river network in the reference maps, in
416 respect to modelled maps. Indeed, the modelling framework excludes river basins with an
417 upstream basin area below 500 km², meaning that EFAS maps only cover main river stems but
418 miss out several smaller tributaries. This is clearly visible over the Severn and in the upper
419 Thames basins (Figure 4), and might also explain the lower skill in the lowlands of Ouse and
420 Trent rivers, where the contributions of main river stems and tributaries to the flood extent are
421 difficult to separate. Including minor tributaries in the flood maps would require either to
422 increase the resolution of the climatological forcing to reproduce intense local rainfall, or to add
423 a pluvial flooding component as done by Wing et al. (2017). Finally, areas prone to storm surge
424 and tidal flooding around river estuaries might further reduce the overall skill of modelled
425 maps, despite the 5km buffer applied.
426

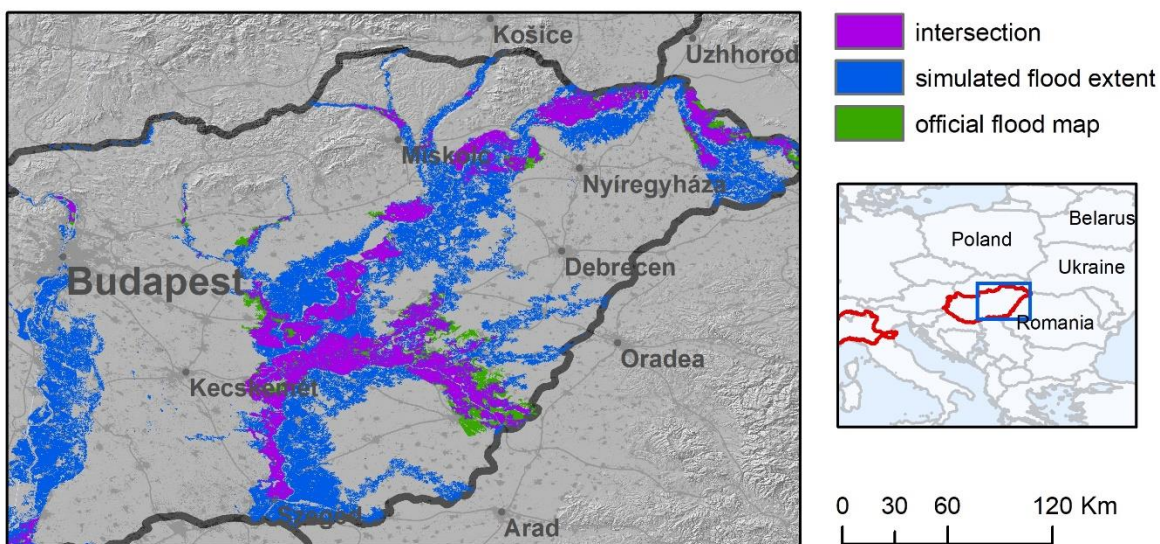


428 *Figure 4. Comparison of modelled (blue) and reference (green) flood hazard maps (1-in-100-*
429 *year) over the Severn (centre) and in the upper Thames basins in England (on the right). Purple*
430 *areas denotes intersection (agreement) between the modelled and reference set of maps. The*
431 *original reference maps (i.e. with no masking around modelled maps) are shown in light green.*
432

433 3.2.2 Hungary

434 The results in Table 3 for Hungary show a general tendency to overestimate flood extent for all
 435 return periods. ~~Hit rate~~HR values are consistently high and do not change much with the return
 436 period. Conversely, ~~false alarm rate~~FAR is very high for the 1-in-30 year flood map and still
 437 considerable even for the 1-in-1000 year flood map. Arnal et al (2019) reported a fair
 438 hydrological skill of LISFLOOD (KGE values >0.5) for the calibration period, even though
 439 KGE validation values were considerably low for the Tisza River.
 440 Given that flood defences are not modelled in reference maps, the observed results may be
 441 explained by assuming a large conveyance capacity of river channels. For instance, the 1-in-100
 442 year reference map show relatively few flooded areas for the Danube main stem (Figure 5), thus
 443 suggesting that the main channels can convey the 1-in-100-year discharge without overflowing.
 444 Conversely, river channels in the modelling framework are assumed to convey only the 1-in-2-
 445 year discharge. Obviously, the same considerations can be made for 1-in-30-year discharge for
 446 the majority of river network, which explains the very low scores. Furthermore, artificial
 447 structures such as road embankments and drainage network may further reduce flood extent in
 448 lowland areas, leading to further overestimation given the fact that these features are not
 449 represented in the DEM. These findings highlight the need for high-resolution DEM fed with
 450 local-scale information to achieve adequate performance in lowland areas, as observed also by
 451 Wing et al (2019b).

452



453 *Figure 5. Comparison of modelled (blue) and reference (green) flood hazard maps (1-in-100-*
454 *year) over the Danube (left) and Tisza (right) rivers in Hungary. Purple areas denotes the*
455 *intersection between the modelled and reference set of maps.*

456

457 3.2.3 Spain

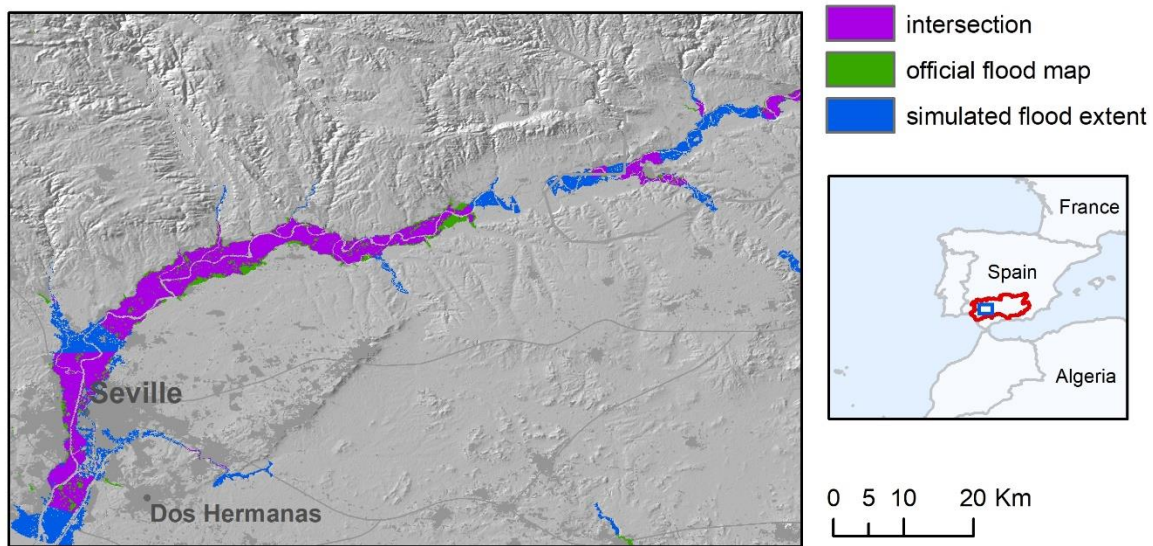
458 The performance of the modelled maps in Spain show a fairly stable HR value and decreasing
459 FAR values with increasing return periods, similarly to what was observed for England and
460 Hungary. The analysis of the results for the major river basins of the Iberian Peninsula, reported
461 in Table 5, provide further insight on the skill of flood maps. A number of basins exhibit both
462 large HR and FAR such as the Duero, Tajo and Guadalquivir basins. Rivers in South-East Spain
463 (Segura, Jucar) have relatively low HR values, while the modelled maps perform better in the
464 Ebro river basin. The interpretation of results requires to consider different aspects. The poor
465 results for the 1-in-10-year maps are likely due to the effect of flood protection structures, such
466 as dykes and flood regulation systems, which are probably relevant also for the 1-in-100-year
467 map. Indeed, most Iberian rivers are regulated by multiple reservoirs, which are often used to
468 reduce flood peaks according to specific operating rules. While dykes are not represented in the
469 inundation model, reservoirs are included in the LISFLOOD model through a simplified
470 approach, given that operating rules are not known. As such, the real and modelled hydrological
471 regimes might differ significantly, including flow peaks of low-probability flood events. This is
472 reflected also by the low hydrological skill of LISFLOOD, with KGE values generally below
473 0.5 with few exceptions (Figure B1).

474 In addition, the comparison of modelled and reference maps is ~~partly~~-affected by the partial
475 coverage of the reference inundation maps in several river basins. According to the information
476 available in the official website (MITECO 2011) large sections of the river network in the
477 basins of the Duero, Tajo, Guadiana and Guadalquivir rivers have not been analyzed, due to the
478 absence of relevant assets or inhabited places at risk. Even though this has been accounted by
479 restricting the area of comparison around reference maps, a visual inspection of the maps being
480 compared shows spurious overestimation around the edges of reference map polygons (Figure
481 6). Finally, the low HR values scored in rivers in South-East Spain (Segura, Jucar) are partially
482 explained by the presence of several tributaries not included in EFAS maps.

483
 484
 485
 486
 487

Catchments	10-year RP			100-year RP			500-year RP		
	HR	FAR	CSI	HR	FAR	CSI	HR	FAR	CSI
Spain	0.58	0.65	0.28	0.63	0.44	0.42	0.61	0.36	0.45
Duero	0.60	0.74	0.22	0.65	0.55	0.36	0.65	0.46	0.42
Ebro	0.71	0.46	0.45	0.75	0.27	0.59	0.74	0.23	0.61
Guadalquivir	0.67	0.66	0.29	0.69	0.49	0.42	0.66	0.46	0.42
Guadiana	0.52	0.63	0.28	0.60	0.42	0.42	0.61	0.31	0.48
Jucar	0.32	0.89	0.09	0.53	0.46	0.36	0.51	0.39	0.39
Tajo	0.60	0.85	0.14	0.70	0.63	0.32	0.69	0.49	0.41
Segura	0.18	0.89	0.07	0.38	0.52	0.27	0.41	0.24	0.36

488 *Table 5. Validation indices in Spain and in some test river basins.*



489
 490 *Figure 6. Comparison of modelled (blue) and reference (green) flood hazard maps (1-in-100-*
 491 *year) over a stretch of the Guadalquivir river basin, Spain. Purple areas denote the intersection*
 492 *between the two set of maps.*

493 3.3 Comparison with previous continental-scale validation studies

494 To put the described outcomes in context, we compare them with the validation exercises
495 performed by Sampson et al. (2015) over the Thames and Severn rivers in England, and by
496 Wing et al. (2017) over United States~~,~~. The study by Wing et al. is, to our knowledge, the only
497 first study that carried out a consistent validation of modelled flood hazard maps at continental
498 scale. Bates et al. (2021) have recently updated the work by Wing et al. by including pluvial and
499 coastal flooding components in the modelling framework, but their work is not considered here.
500 A comparison of validation metrics of the three studies are shown in Table 6 and 7. For our
501 framework, we calculated each index in Table 6 using the overall modelled and reference flood
502 extent available for each return period (e.g. the value for the 100-year maps includes reference
503 and modelled maps for England, Spain and Norway). As such, each area is weighted according
504 to the extent of the corresponding flood map.

505 As can be seen in Table 6, the continental-scale model by Wing et al. achieved the highest
506 scores both for 100y and 500y return periods. However, this model is based on national datasets
507 with higher accuracy and resolution than those available for the European continent (e.g. a 10m-
508 resolution DEM and a detailed catalogue of flood defences). The global and European models
509 have comparable hit rates for the 100-year flood maps (0.68 and 0.65 respectively), but the
510 former exhibits a much lower FAR value (0.34 compared to 0.61 of the European model), and a
511 higher HR value for the 500-year maps.

512 The higher HR values scored by the US and global models might depend on the higher density
513 of the modelled river network, which includes river reaches up to 50km² by simulating both
514 pluvial and fluvial flooding processes. The lower FAR values of the US and global models
515 might be explained by the inclusion of flood defences. In the US model, defences are explicitly
516 modelled using the US dataset of flood defences, while the global model parameterizes flood
517 defences through the adjustment of channel conveyance using socioeconomic factors and degree
518 of urbanization (Wing et al., 2017). However, Wing et al observed that the latter methodology
519 had a negligible effect on hit rates in defended areas, when compared against an undefended
520 version of the model.

521 Another possible reason for the low FAR values is the different approach used in the validation
522 method. Wing et al. applied a narrow 1km buffer around official maps to constrain the area of
523 comparison and avoid spurious over-prediction in areas not considered by official maps.

524 However, this might result in a reduction of true false alarms, because part of overestimated
 525 flood areas can go undetected. To verify this hypothesis, we recalculated the performance
 526 indices against the 100-year reference map in Spain using a 1km buffer instead of the 5km
 527 previously applied to constrain the validation area. As a result the false alarm ratio dropped
 528 from 0.44 to 0.34, similar to the performance of the global model. However, we observed a
 529 reduction of true false alarms, especially in river basins with continuous map coverage such as
 530 the Ebro, Jucar and Segura.

531

	RP	HR	FAR	CSI
US model (Wing et al.)	100	0.82	0.37	0.55
Global model (Wing et al.)	100	0.69	0.34	0.50
European model (this study)	100	0.66	0.61	0.32
US model (Wing et al.)	500	0.86	na	na
Global model (Wing et al.)	500	0.74	na	na
European model (this study)	500	0.61	0.24	0.51
European model (this study)	1000	0.68	0.39	0.47

532 *Table 6. Comparison of the performance metrics for the European model described in the*
 533 *present study and the two models evaluated in the study by Wing et al. (2017).*

534

535 The comparison of HR, FAR and CSI values show better scores for the global maps by
 536 Sampson et al. (2015) in respect to our modelled maps (Table 7).

537

	<u>HR</u>	<u>FAR</u>	<u>CSI</u>
<u>Thames (this study)</u>	<u>0.56</u>	<u>0.46</u>	<u>0.38</u>
<u>Thames (Sampson et al. 2015)</u>	<u>0.73</u>	<u>0.3</u>	<u>0.56</u>
<u>Severn (this study)</u>	<u>0.64</u>	<u>0.24</u>	<u>0.53</u>
<u>Severn (Sampson et al. 2015)</u>	<u>0.83</u>	<u>0.23</u>	<u>0.67</u>

538 *Table 7. Comparison of the performance metrics for the maps described in the present study*
 539 *and the global maps by Sampson et al. (2015). Metrics for the latter study are calculated*
 540 *removing all channels with upstream areas of less than 500 km².*

541

542 The different masking applied to reference flood maps may explain some of the differences:
 543 Sampson et al. removed all channels with upstream areas of less than 500 km², whereas here we
 544 use a simpler 5km buffer around modelled maps. The exclusion of permanent river channels in
 545 our comparison may further penalize the overall score especially for the Thames, which as a
 546 rather large channel estuary. Besides these differences in the validation, the better metrics of the
 547 maps by Sampson et al. may depend on a more accurate hydrological input (based on
 548 regionalization of gauge station data) and a better correction of urban elevation bias (based on a
 549 moving window filter instead of the constant correction values applied here).

550 To provide further context, the US model by Wing et al. (2017) attained average CSIs of ~0.75
 551 against a number of detailed local models, whereas flood models built and calibrated for local
 552 applications may achieve CSI scores up to 0.9 when benchmarked against very high quality data
 553 (see Wing et al., 2019a). Fleischmann et al. (2019) recently proposed that regional-scale models
 554 can provide locally relevant estimates of flood extent when $CSI > 0.65$. Although the overall
 555 values shown in Table 3 are consistently below this threshold, better results are observed for a
 556 number of river basins, as shown in Tables 4 and 5.

557

558 *3.4 Comparison with the previous flood map dataset*

559 Table 7 compares the performances of the flood hazard maps described in the present study
 560 (version 2) with the previous version developed by Dottori et al. (2016a; version 1). The
 561 comparison is shown for England and Hungary. Results for all other areas are comprised within
 562 the range of results shown in Table 3. As can be seen, differences are generally reduced across
 563 the different areas and return periods. Version 1 of the flood maps produced slightly better
 564 results in Hungary for the 100- and 1000-year return period (increased CSI and HR, lower
 565 FAR), while version 2 has somewhat improved performances in England, mainly driven by
 566 higher HR.

	RP (y)	F2/F1	ΔHR	ΔFAR	ΔCSI
Hungary	30	0.97	-0.5%	-0.4%	2.9%
Hungary	100	1.00	-2.1%	0.7%	-2.4%
Hungary	1000	1.01	-3.6%	5.7%	-6.3%
England	100	1.05	9.4%	1.7%	7.3%

England	1000	1.04	8.2%	-1.1%	7.7%
---------	------	------	------	-------	------

567 *Table 7. Comparison of performances of the flood hazard maps described in the present study*
568 *and developed by Dottori et al. (2016a). Table reports the ratio between flood extents (F2/F1)*
569 *and the difference between version 2 and 1 of the HR, CSI, FAR values.*

570

571 These outcomes may be interpreted considering the changes in input data between the two
572 versions, and the structure of the modelling approach and of input data, which in turn has not
573 changed substantially. The main difference between the two map versions is given by the
574 hydrological input, with version 2 using the latest calibrated version of the LISFLOOD model.

575 For the 100-year return period, peak flow values of version 2 are on average 35% lower than
576 version 1 in Hungary, and 16% lower in England. However, similar decreases are also observed
577 for the 1-in-2-year peak discharge which determines bankful discharge. The resulting reduction
578 in channel hydraulic conveyance in respect to version 1 is likely to offset the decrease of peak
579 flood volumes, which explain the small difference in overall flood extent given by the F2/F1
580 parameter in table 7. Such result confirm that the knowledge of river channel geometry is
581 crucial to correctly model the actual channel conveyance and thus improve inundation
582 modelling. Other differences in input data are given by minor changes in Manning's parameters
583 and in the EFAS river network, which might contribute to the observed differences.

584

585 *3.5 Influence of elevation data*

586 Table 8 compares the metrics calculated with CCM DEM elevation data against the same
587 metrics for the modelled flood maps based on MERIT-DEM. The comparison is carried out for
588 England, Hungary and the Po river basin. Performance is slightly improved by the use of
589 MERIT-DEM data for all areas and return periods, in particular through the reduction of FAR,
590 even though the overall increase of CSI values is limited to few percentage points.

591

	RP (y)	ΔF	ΔHR	ΔFAR	ΔCSI
Hungary	100	-5.3%	0.0%	-2.0%	5.1%
Hungary	1000	-5.9%	-0.1%	-7.6%	5.2%
England	100	0.0%	2.6%	-5.7%	3.8%

England	1000	1.7%	2.8%	-7.8%	3.2%
Po	500	0.2%	0.9%	-4.3%	3.4%

592 *Table 8. Comparison of performances of the flood hazard maps described in the present study*
593 *and developed by Dottori et al. (2016a based on the MERIT-DEM (a) and CCM-DEM (b).*
594 *Table reports the ratio between flood extents F and the differences for HR, CSI, FAR (e.g. ($HRa -$*
595 *$HRb)/HRa$).*

596

597 Because of this limited improvement and the considerable amount of time required to rerun the
598 complete set of flood hazard maps (several days for each return period) it was decided not to
599 update the flood maps using the MERIT-DEM as elevation data. Moreover, new high-resolution
600 datasets such as the Copernicus DEM (ESA-Airbus 2019), [the 90m version of TanDEM-X](https://geoservice.dlr.de/web/dataguide/tdm90)
601 [dataset \(https://geoservice.dlr.de/web/dataguide/tdm90\)](https://geoservice.dlr.de/web/dataguide/tdm90), and MERIT-HYDRO (Yamazaki et
602 al., 2019) have recently become available, and therefore future research could focus on
603 performing additional comparisons to identify which dataset is most suitable for inundation
604 modelling in Europe.

605

606 **4) Conclusions and ongoing work**

607 We presented here a new dataset of flood hazard maps covering the geographical Europe and
608 including large parts of the Middle East and river basins entering the Mediterranean Sea. This
609 dataset significantly expands the previous available flood maps datasets at continental scale
610 (Alfieri et al., 2014; Dottori et al., 2016a), and therefore constitutes a valuable source of
611 information for future research studies and flood management, especially for countries where no
612 official flood hazard maps are available. [The new maps also benefit of updated models and new](#)
613 [calibration and meteorological data.](#) The maps are being used for a range of applications at
614 continental scale, from evaluating present and future river flood risk scenarios, to the cost-
615 benefit assessment of different adaptation strategies to reduce flood impacts, and for
616 comparisons between different regions, countries and river basins (Dottori et al, 2020b).
617 Moreover, the flood hazard maps [are](#) designed to be integrated with the European Flood
618 Awareness System (EFAS), and will be used to perform operational flood impact forecasting in
619 EFAS (Dottori et al., 2017).

620 We performed a detailed validation of the modelled flood maps in several European countries
621 against official flood hazard maps. The resulting validation exercise is the most complete
622 undertaken so far for Europe to our best knowledge, and provided a comprehensive overview of
623 the strengths and limitations of the new maps. Nevertheless, the unavailability of reference
624 flood maps outside Europe did not allow any validation in the arid regions in North Africa and
625 Eastern Mediterranean. In these areas, further research will be needed to better understand the
626 performance of the flood mapping procedure here proposed.

627 Modelled maps generally achieve low scores for high and medium probability of flooding. For
628 the 1-in-100-year flood probability, the modelled maps can identify on average two-thirds of
629 reference flood extent, however they also largely overestimate flood-prone areas in many
630 regions, thus hampering the overall performance. Performances improves markedly with the
631 increasing of return period, mostly due to the decrease of the false alarm rates. In particular,
632 critical success index (CSI) values approach and in some cases exceed 0.5 for return periods
633 equal or above 500 years, meaning that the maps can correctly identify more than half of
634 flooded areas in the main river stems and tributaries of different river basins.

635 It is important to note that the validation was affected by problems in identifying the correct
636 areas for a fair comparison, because of the different density of the mapped river network in
637 reference and modelled maps. In our study we opted for a conservative approach using large
638 buffers to constrain comparison areas, which possibly penalized the model performance, e.g.
639 due to spurious false alarms in areas not considered by official maps. However, we observed
640 that the proposed maps achieve comparable results to other large-scale flood models when using
641 similar parameters for the validation.

642 The low skill of modelled maps for high and medium probability of flooding, with large
643 overestimations observed in different lowland areas, is mostly motivated by the non-inclusion
644 of flood defences in the modelling framework and the simplified representation of channel
645 hydraulic conveyance, due to the absence of datasets at European scale describing river
646 channels and defence structures (i.e. design standards and location of dyke systems). Such
647 information combined with high-resolution DEM fed with local-scale information (artificial and
648 defence structures) is crucial to improve the performance of large-scale flood models and apply
649 more realistic flood modelling tools, as observed also by Wing et al (2017, 2019b). On this
650 point, we found that the modelling approach has limited sensitivity to changes in the

651 hydrological input, because channel conveyance is linked to streamflow characteristics. Such
652 finding highlight the need for independent data of river channel width, shape and depth to better
653 reproduce streamflow and flooding processes. Moreover, the improved results offered by the
654 use of the MERIT-DEM elevation data suggest that recent high-resolution datasets such as the
655 Copernicus DEM (ESA-Airbus 2019), [TanDEM-X](https://www.copernicus.eu/en/tandem-x)
656 (<https://geoservice.dlr.de/web/dataguide/tm90>), and MERIT-HYDRO (Yamazaki et al., 2019)
657 may offer a viable solution to improve future versions of continental-scale flood hazard maps in
658 Europe.

659 Increasing map coverage by including the minor river network is likely to improve the skill of
660 modelled maps. However, this might require the use of a different modelling approach to
661 account for pluvial flooding (Wing et al., 2017; [Bates et al., 2021](#)), along with reliable model
662 climatology to represent small-scale precipitation processes. Improving the simulation of
663 reservoirs may also reduce the difference between the real and modelled hydrological regimes
664 in regions such as the Iberian Peninsula and the Alps.

665

666 *Data availability*

667 The dataset described in this manuscript is accessible as part of the data collection “Flood
668 Hazard Maps at European and Global Scale” at the JRC data Catalogue
669 (<https://data.jrc.ec.europa.eu/collection/floods/>).

670 Please refer to the dataset as follows: Dottori F., Bianchi A., Alfieri, L., Skoien, J., Salamon P.,
671 2020. River flood hazard maps for Europe and the Mediterranean Basin region. JRC Data
672 Catalogue, accessible at <http://data.europa.eu/89h/1d128b6c-a4ee-4858-9e34-6210707f3c81>,
673 [doi: 10.2905/1D128B6C-A4EE-4858-9E34-6210707F3C81](https://doi.org/10.2905/1D128B6C-A4EE-4858-9E34-6210707F3C81).

674 Note that the DOI for the dataset will be available soon. The dataset comprises the following
675 eight maps, each one available as GEOTIF file:

- 676 • Map of permanent water bodies for Europe and the Mediterranean Basin region
- 677 • River network in Europe and the Mediterranean Basin region
- 678 • River flood hazard maps for Europe and the Mediterranean Basin region (return periods of
679 10, 20, 50, 100, 200 and 500 years)

680 The official flood hazard maps used for the validation exercise are freely accessible at the
681 following websites:

- 682 • Spain: <https://www.miteco.gob.es/es/cartografia-y-sig/ide/descargas/agua/zi-lamina.aspx>
683 (in Spanish)
- 684 • Po River Basin: <https://pianoalluvioni.adbpo.it/progetto-esecutivo-delle-attivita/> (in
685 Italian)
- 686 • Norway: <https://www.nve.no/flaum-og-skred/kartlegging/flaum/> (in Norwegian)
- 687 • England: [https://data.gov.uk/dataset/bed63fc1-dd26-4685-b143-2941088923b3/flood-](https://data.gov.uk/dataset/bed63fc1-dd26-4685-b143-2941088923b3/flood-map-for-planning-rivers-and-sea-flood-zone-3)
688 [map-for-planning-rivers-and-sea-flood-zone-3](https://data.gov.uk/dataset/cf494c44-05cd-4060-a029-35937970c9c6/flood-map-for-planning-rivers-and-sea-flood-zone-2) ; [https://data.gov.uk/dataset/cf494c44-](https://data.gov.uk/dataset/cf494c44-05cd-4060-a029-35937970c9c6/flood-map-for-planning-rivers-and-sea-flood-zone-2)
689 [05cd-4060-a029-35937970c9c6/flood-map-for-planning-rivers-and-sea-flood-zone-2](https://data.gov.uk/dataset/cf494c44-05cd-4060-a029-35937970c9c6/flood-map-for-planning-rivers-and-sea-flood-zone-2)
- 690 • Hungary: <https://www.vizugy.hu/index.php?module=content&programelemid=62> (in
691 Hungarian)

692 The LISFLOOD hydrological model used in this research is released as open-source software
693 and available at <https://ec-jrc.github.io/lisflood/>.

694 The LISFLOOD-FP hydrodynamic model used in this research can be requested to the authors
695 for research and non-commercial purposes at
696 <http://www.bristol.ac.uk/geography/research/hydrology/models/lisflood/>
697

698 ***Appendix A: meteorological observations used for LISFLOOD simulations***

699 The long-term run of the hydrological model LISFLOOD is based on observed data from
700 meteorological stations and precipitation datasets, which are collected and continuously
701 expanded as part of the development work for EFAS. The meteorological variables considered
702 are: precipitation, minimum and maximum temperature, wind speed, solar radiation and vapour
703 pressure. The number of stations with available meteorological observations depends on the
704 period and variable considered, with an increasing availability towards the end of the historical
705 simulation period. As an example, for the year 2016 the number of daily observations available
706 ranged from ~8.800 for temperature to ~5.500 for precipitation and ~3.700 for vapour pressure.
707 The input from meteorological stations is completed by a number of precipitation datasets
708 (EURO4M-APG, INCA-Analysis Austria, ERA-Interim GPCP corrected and Carpat-Clim; for
709 details see Arnal et al., 2019). Note that the same datasets are used to drive the LISFLOOD

710 calibration and to calculate the initial conditions for the EFAS forecasts. The data from
711 meteorological stations and gridded datasets were then interpolated using the interpolation
712 scheme SPHEREMAP to produce meteorological grids with a daily time step. The reader is
713 referred to Arnal et al. (2019) for further details.
714

715 *Appendix B: LISFLOOD calibration results*

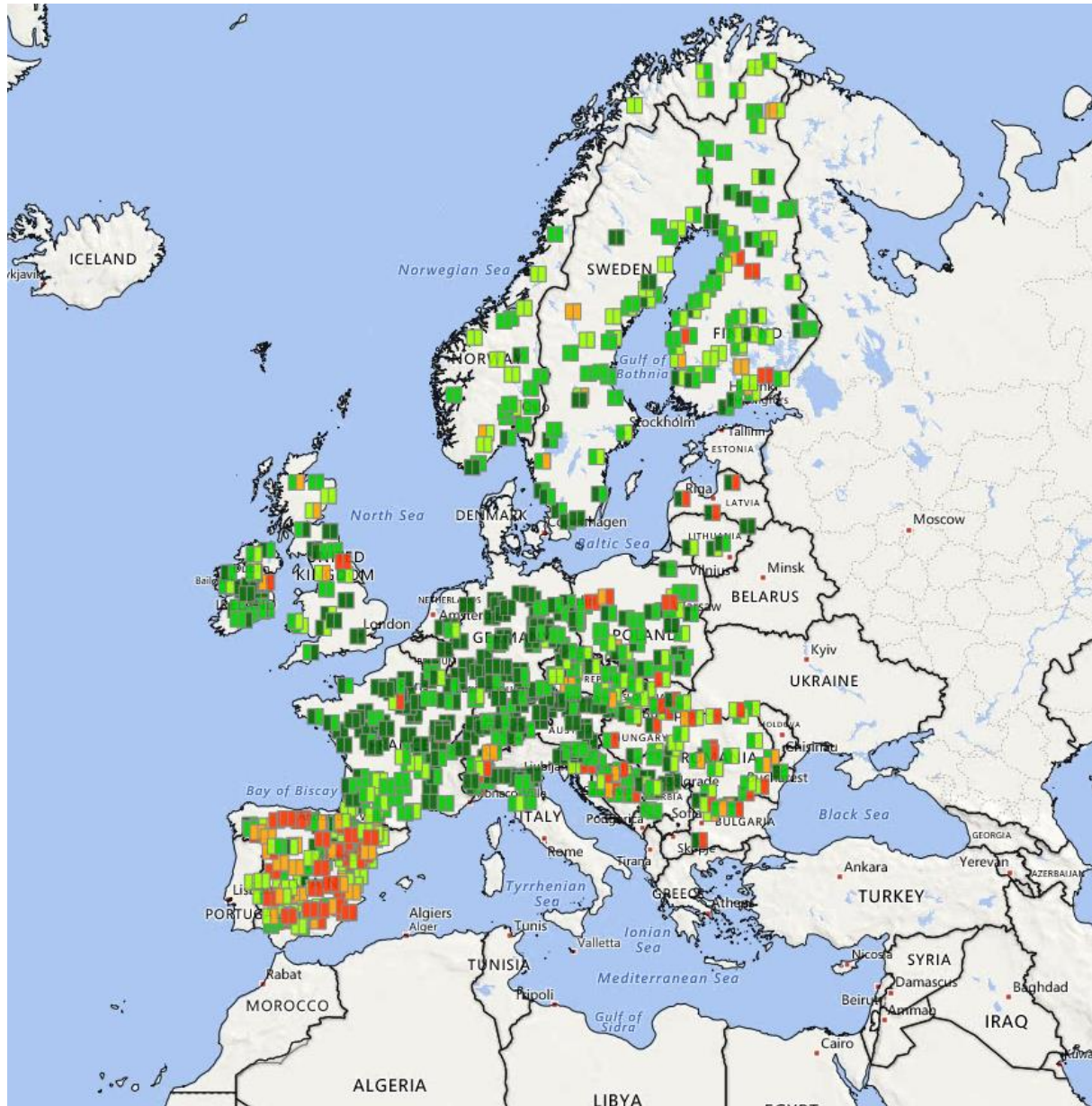
716 We report here the results of the LISFLOOD calibration presented by Arnal et al. (2019). The
717 hydrological skill of LISFLOOD is expressed by the Kling-Gupta Efficiency (KGE, Gupta et
718 al., 2009). Figure B1 shows the spatial distribution of the hydrological skill across the EFAS
719 domain. 75 % of all stations (543 out of 717) scored a KGE higher than 0.5 during calibration,
720 and 57 % (409 out of 698) during validation.

721 It is clearly noticeable that the skill is not homogeneously distributed across Europe, with higher
722 skills in large parts of Central Europe, and lower skill mostly in Spain caused by the strong
723 influence of reservoirs. The other study areas considered in the validation exercise (England,
724 Hungary, Norway, Po river basin) exhibit KGE values generally above 0.5.

725 *Appendix C: Additional results*

726 *C1: validation results for the Po River Basin*

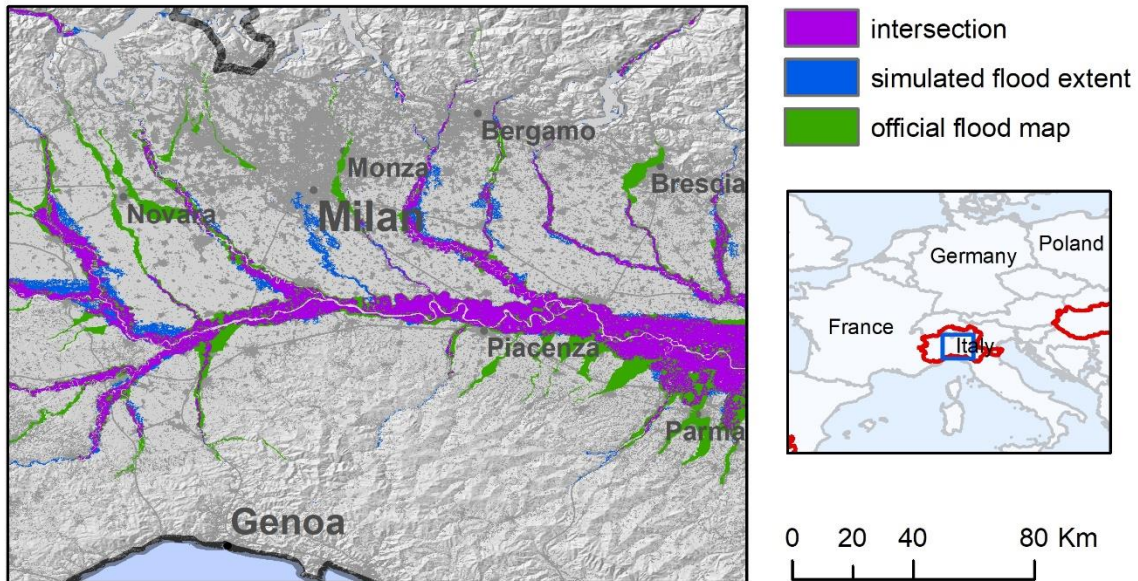
727 According to Table 3, the modelled flood maps provide a better reproduction of reference maps
728 for the Po River, compared to other study areas. False alarms are low, while hit ratio (HR)
729 values indicate that two out of every three pixels in the reference map are correctly identified as
730 flooded. The analysis of reference and modelled maps (Figure C1), suggests that the
731 underestimation is partly caused by flooded areas along some tributaries which are not included
732 in modelled maps. Other areas with omission errors are located near confluences of the Po main
733 stem and the major tributaries in Emilia-Romagna, which may depend on the underestimation of
734 peak flow on tributaries. In fact, the results of the LISFLOOD calibration in Figure B1 show
735 better hydrological skill along the Po main stem, compared to some tributaries. Finally, it is
736 likely that the inclusion of smaller tributaries of the river network in the modelled maps would
737 improve the overall performance.



739

740 *Figure B1. Hydrological skill of EFAS at the calibration locations. Colour coding denotes the*
 741 *quality of the KGE during calibration (left half of square) and validation (right half of the*
 742 *square). Dark green: $KGE > 0.75$; Green: $KGE 0.5 - 0.75$, Light green: $KGE 0.2 - 0.5$;*
 743 *Orange: $0 - 0.2$; Red: < 0 . Source: Arnal et al. (2019).*

744



745
 746 *Figure C1. Comparison of modelled (blue) and reference (green) flood hazard maps (1-in-500-*
 747 *year) over the Po river basin, Italy. Purple areas denotes the intersection (agreement) between*
 748 *the two set of maps.*

749

750 ***C2: validation results for Norway***

751 The results of the modelled flood maps in Norway show a general tendency to overestimate
 752 flood extent for the 1-in-100-year events, with high values for both hit ratio (HR) and false
 753 alarm ratio (FAR). Such a result is in fact largely influenced by the relatively small extent and
 754 discontinuous coverage of reference maps. Flood-prone areas for the 1-in-100-year official
 755 maps only cover 215 km², possibly due to the low density of populated places in Norway, while
 756 they cover between 4700 and 5700 km² for England, Spain and Hungary. As for Spain, we
 757 applied a 5km buffer to restrict the area of comparison around reference maps, yet this leads to
 758 spurious overestimation around the edges of reference map polygons. Notably, the performance
 759 improves markedly with the use of a 1km buffer as in Wing et al., (2017), which results in
 760 increased critical success index (CSI) scores up to nearly 0.50.

761 The results of reported by Arnal et al. (2019) and summarized in Figure B1 suggest an
 762 acceptable hydrological skill of the LISFLOOD calibration in Norway, with a majority of gauge
 763 stations scoring KGE values above 0.5. In the areas with lower scores, the model performance
 764 for low-probability flood events might be influenced by an incorrect estimation of peak

765 discharges driven by snow melt, which plays a relevant role in determining low-probability
766 flood events.

767

768 ***C3: Influence of correcting elevation data with land use***

769 We tested the results of correcting CCM DEM elevation data with vegetation cover in
770 Scandinavia, where the percentage of land covered by forests is more relevant than in the other
771 regions included in the modelled flood maps. For the 1-in100-year flood maps, the overall
772 difference in flood extent between the corrected and uncorrected maps is less than 4%, and
773 similar values were found for the other return periods. Moreover, the HR, FAR and CSI values
774 of two set of maps differ by less than 2% when calculated against the 1-in100-year official map
775 in Norway, probably because forested areas have not been considered as relevant flood-prone
776 areas. These results suggest that the simulation of densely vegetated areas have a limited
777 importance in determining the overall performance of modelled flood maps in Europe.

778

779 ***Author contribution***

780

781 FD: conceptualization, formal analysis, investigation, data curation writing (original draft,
782 review and editing); LA: methodology, investigation, writing (review and editing); AB: data
783 curation, validation, visualization; JS: investigation, writing (review and editing); PS:
784 conceptualization, project administration, writing (original draft, review and editing)

785

786 ***Competing interests***

787 The authors declare that they have no conflict of interest.

788

789 ***Acknowledgements***

790 This study has been partially funded by the COPERNICUS programme and by an
791 administrative arrangement with Directorate General 'European Civil Protection and

792 Humanitarian Aid Operations (DG ECHO) of the European Commission. EFAS is operated and
793 financed as part of the Copernicus Emergency Management Service.

794

795

796 *References*

797 Alfieri, L., Salamon, P., Bianchi, A., Neal, J., Bates, P.D., Feyen, L., 2014. Advances in pan-
798 European flood hazard mapping, *Hydrol. Process.*,28 (18), 4928-4937, doi:10.1002/hyp.9947.

799 Alfieri L., Feyen L., Dottori F., Bianchi A., 2015. Ensemble flood risk assessment in Europe
800 under high end climate scenarios. *Global Environmental Change* 35, 199–212.

801 Alfieri, L., L. Feyen, and G. D. Baldassarre (2016), Increasing flood risk under climate
802 change: a pan-European assessment of the benefits of four adaptation strategies, *Clim. Change*,
803 136(3), 507–521, doi:10.1007/s10584-016-1641-1.

804 Arnal, L., S.-S. Asp, C. Baugh, A. de Roo, J. Disperati, F. Dottori, R. Garcia, M.
805 GarciaPadilla, E. Gelati, G. Gomes, M. Kalas, B. Krzeminski, M. Latini, V. Lorini, C. Mazzetti,
806 M. Mikulickova, D. Muraro, C. Prudhomme, A. Rauthe-Schöch, K. Rehfeldt, P. Salamon, C.
807 Schweim, J.O. Skoien, P. Smith, E. Sprokkereef, V. Thiemig, F. Wetterhall, M. Ziese, 2019.
808 EFAS upgrade for the extended model domain – technical documentation, EUR 29323 EN,
809 Publications Office of the European Union, Luxembourg, 2019, ISBN 978-92- 79-92881-9, doi:
810 10.2760/806324, JRC111610.

811 Bates, P. D., De Roo, A. P. J., 2000. A simple raster-based model for flood inundation
812 simulation, *J. Hydrol.*, 236 (1–2), 54–77.

813 Bates P.D., Horritt M.S., and Fewtrell T.J., 2010. A simple inertial formulation of the
814 shallow water equations for efficient two-dimensional flood inundation modelling. *Journal of*
815 *Hydrology*, 387, 33-45.

816 [Bates, P. D., Quinn, N., Sampson, C., Smith, A., Wing, O., Sosa, J., et al. \(2021\). Combined](#)
817 [modeling of US fluvial, pluvial, and coastal flood hazard under current and future climates.](#)
818 [Water Resources Research, 57, e2020WR028673. https://doi.org/10.1029/2020WR028673](#)

819 Baugh, C. A., Bates, P. D., Schumann G., Trigg, M.A., 2013. SRTM vegetation removal
820 and hydrodynamic modeling accuracy, *Water Resour. Res.* 49, 5276–5289,
821 doi:10.1002/wrcr.20412.

822 Barredo JJ, de Roo A, Lavalle C. 2007. Flood risk mapping at European scale. *Water*
823 *Science and Technology* 56: 11–17.

824 Bontemps, S., et al., 2009. GLOBCOVER -Products description and validation report, Univ.
825 Catholique de Louvain.

826 Burek, P., Knijff van der, J., Roo de, A., 2013. LISFLOOD, Distributed Water Balance and
827 Flood Simulation Model Revised User Manual 2013. Publications Office, Luxembourg.

828 Copernicus Land Monitoring Service. Corine Land Cover. [http://land.copernicus.eu/pan-](http://land.copernicus.eu/pan-european/corine-land-cover)
829 [european/corine-land-cover](http://land.copernicus.eu/pan-european/corine-land-cover) (accessed on 12/2/2020).

830 Dottori, F., Alfieri, L., Salamon, P., Bianchi, A., Feyen, L., Lorini, V., 2016a: Flood hazard
831 map for Europe - 100-year return period. European Commission, Joint Research Centre (JRC)
832 [Dataset] PID: http://data.europa.eu/89h/jrc-floods-floodmapeu_rp100y-tif

833 Dottori, F., Salamon, P., Bianchi, A., Alfieri, L., Hirpa, F.A., Feyen, L., 2016b.
834 Development and evaluation of a framework for global flood hazard mapping. *Advances in*
835 *Water Resources* 94, 87–102.

836 Dottori F., Kalas M., Salamon P., Bianchi A., Alfieri, L., Feyen L., 2017. An operational
837 procedure for rapid flood risk assessment in Europe. *Nat. Hazards Earth Syst. Sci.*, 17, 1111-
838 1126, <https://doi.org/10.5194/nhess-17-1111-2017>.

839 Dottori, F., Szewczyk, W., Ciscar, J.C., Zhao, F., Alfieri, L., Hirabayashi, Y., Bianchi, A.,
840 Frieler, K., Betts, R.A., Feyen, L., 2018 Increased human and economic losses from river floods
841 with anthropogenic warming. *Nature Climate Change*, 8(9), 781-786,
842 <https://doi.org/10.1038/s41558-018-0257-z>

843 Dottori F., Bianchi A., Alfieri, L., Skoien, J., Salamon P., 2020a. River flood hazard maps
844 for Europe and the Mediterranean Basin region. JRC Data Catalogue, accessible at
845 <https://data.jrc.ec.europa.eu/dataset/1d128b6c-a4ee-4858-9e34-6210707f3c81> .

846 Dottori F, Mentaschi L, Bianchi A, Alfieri L and Feyen L, 2020b. Adapting to rising river
847 flood risk in the EU under climate change, EUR 29955 EN, Publications Office of the European
848 Union, Luxembourg, 2020, ISBN 978-92-76-12946-2 , doi:10.2760/14505, JRC118425.

849 European Commission (EC), 2007. Directive 2007/60/EC of the European
850 Parliament and of the Council on the assessment and management of flood risks,
851 Official Journal of the European Communities, Brussels, available at: [http://eur-](http://eur-lex.europa.eu/legal-content/EN/TXT/?uri=CELEX%3A32007L0060)
852 [lex.europa.eu/legal-content/EN/TXT/?uri=CELEX%3A32007L0060](http://eur-lex.europa.eu/legal-content/EN/TXT/?uri=CELEX%3A32007L0060) (accessed on 13/5/2020).

853 ESA-Airbus, 2019. Copernicus Digital Elevation Model Validation Report, accessed on
854 14/5/2020 at [https://spacedata.copernicus.eu/documents/12833/20611/GEO1988-](https://spacedata.copernicus.eu/documents/12833/20611/GEO1988-CopernicusDEM-RP-001_ValidationReport_V1.0/9bc5d392-c5f2-4118-bd60-db9a6ea4a587)
855 [CopernicusDEM-RP-001_ValidationReport_V1.0/9bc5d392-c5f2-4118-bd60-db9a6ea4a587](https://spacedata.copernicus.eu/documents/12833/20611/GEO1988-CopernicusDEM-RP-001_ValidationReport_V1.0/9bc5d392-c5f2-4118-bd60-db9a6ea4a587)

856 Feyen L, Dankers R, Bódis K, Salamon P, Barredo JI. 2012. Fluvial floodrisk in Europe in
857 present and future climates. *Climatic Change*: 112(1): 47–62, doi:10.1007/s10584-011-0339-7.

858 Fleischmann A., R. Paiva, W. Collischonn, 2019. Can regional to continental river
859 hydrodynamic models be locally relevant? A cross-scale comparison. *Journal of Hydrology X*,
860 2019.

861 Gupta, H.V., H. Kling, K.K. Yilmaz, G.F. Martinez, 2009: Decomposition of the mean
862 squared error and NSE performance criteria: implications for improving hydrological
863 modelling. *Journal of Hydrology*, 377, 80-91.

864 Hirpa, F.A.; Salamon, P.; Beck, H.E.; Lorini, V.; Alfieri, L.; Zsoter, E.; Dadson, S.J. , 2018.
865 Calibration of the Global Flood Awareness System (GloFAS) using daily streamflow data. *J.*
866 *Hydrol.*, 566, 595–606.

867 Jongman, B., Hochrainer-Stigler, S., Feyen, L., Aerts, J.C.J.H., Mechler, R., Botzen,
868 W.J.W., Bouwer, L.M., Pflug, G., Rojas, R., Ward, P.J., 2014. Increasing stress on disaster-risk
869 finance due to large floods. *Nat. Clim. Change* 4, 264-268,
870 doi:<http://dx.doi.org/10.1038/nclimate2124>.

871 [Kulp, S.A.; Strauss, B.H. CoastalDEM: A global coastal digital elevation model improved](#)
872 [from SRTM using a neural network. *Remote Sens. Environ.* 2018, 206, 231–239.](#)

873 [Liu, Y., Bates, P.D., Neal, J.C. and Yamazaki, D., 2019, December. Bare-earth DEM](#)
874 [Generation in Urban Areas Based on a Machine Learning Method. In *AGU Fall Meeting*](#)
875 [Abstracts \(Vol. 2019, pp. H41N-1899\).](#)

876 [Meadows, M.;Wilson, M. A Comparison of Machine Learning Approaches to Improve Free](#)
877 [Topography Data for Flood Modelling. *Remote Sens.* 2021, 13, 275.](#)
878 <https://doi.org/10.3390/rs13020275>

879 Ministerio de Medio Ambiente y Medio Rural y Marino (MITECO), 2011. Guía
880 Metodologica para el desarrollo del sistema nacional de cartografía de zonas inundables.
881 Accessed on 18/5/2020 at [https://www.miteco.gob.es/es/agua/temas/gestion-de-los-riesgos-de-](https://www.miteco.gob.es/es/agua/temas/gestion-de-los-riesgos-de-inundacion/snczi/Guia-metodologica-determinacion-zonas-inundables/default.aspx)
882 [inundacion/snczi/Guia-metodologica-determinacion-zonas-inundables/default.aspx](https://www.miteco.gob.es/es/agua/temas/gestion-de-los-riesgos-de-inundacion/snczi/Guia-metodologica-determinacion-zonas-inundables/default.aspx) (in Spanish).

883 The Norwegian Water Resources and Energy Directorate, 2020. Flood Zone Maps.
884 Accessed on 24/4/2020 at <https://www.nve.no/flaum-og-skred/kartlegging/flaum/> (in
885 Norwegian)

886 Paprotny, D., Morales-Nápoles, O., and Jonkman, S. N.: Efficient pan-European river flood
887 hazard modelling through a combination of statistical and physical models, *Nat. Hazards Earth*
888 *Syst. Sci.*, 17, 1267-1283, <https://doi.org/10.5194/nhess-17-1267-2017>, 2017.

889 Sampson, C. C., Smith, A. M., Bates, P. D., Neal, J. C., Alfieri, L., & Freer, J. E. (2015). A
890 high-resolution global flood hazard model. *Water Resources Research*, 51(9), 7358-7381.

891 Scussolini, P., Aerts, J. C. J. H., Jongman, B., Bouwer L. M., Winsemius H. C., de Moel H.,
892 and Ward, P. J., 2015. FLOPROS: an evolving global database of flood protection standards.
893 *Nat. Hazards Earth Syst. Sci. Discuss.*, 3, 7275–7309, 2015, doi:10.5194/nhessd-3-7275-2015.

894 [Shaw, J., Kesserwani, G., Neal, J., Bates, P., and Sharifian, M. K.: LISFLOOD-FP 8.0: the](#)
895 [new discontinuous Galerkin shallow-water solver for multi-core CPUs and GPUs, *Geosci.*](#)
896 [Model Dev.](#), 14, 3577–3602, <https://doi.org/10.5194/gmd-14-3577-2021>, 2021.

897 Thielen J., Bartholmes J., Ramos M.H., and De Roo A. (2009). The European flood alert
898 system - part 1: concept and development. *Hydrol. Earth Syst. Sci.* 13, 125-140.

899 Trigg, M. et al., 2016. The credibility challenge for global fluvial flood risk analysis.
900 *Environ. Res. Lett.* 11 094014

901 United Nations Office for Disaster Risk Reduction (UNISDR), 2015. Sendai Framework for
902 Disaster Risk Reduction 2015–2030 (www.unisdr.org/we/inform/publications/43291)

903 Van der Knijff, J.M., Younis, J., de Roo, A.P.J., 2010. LISFLOOD: a GIS-based
904 distributed model for river basin scale water balance and flood simulation. *Int. J. Geogr. Inf. Sci.*
905 24, 189-212.

906 Vogt et al., 2007. A pan-European river and catchment database, JRC Reference Reports,
907 doi:0.2788/35907.

908 Ward, P.J. et al., 2015. Usefulness and limitations of global flood risk models. *Nature*
909 *Climate Change* 5, 712–715.

910 [Wendi, D.; Liang, S.-Y.; Sun, Y.; Doan, C.D. An innovative approach to improve SRTM](#)
911 [DEM using multispectral imagery and artificial neural network. *J. Adv. Model. Earth Syst.*](#)
912 [2016, 8, 691–702.](#)

913 Wing, O. E., Bates, P. D., Sampson, C. C., Smith, A. M., Johnson, K. A., & Erickson, T. A.
914 (2017). Validation of a 30 m resolution flood hazard model of the conterminous United States.
915 *Water Resources Research*, 53(9), 7968-7986, doi:10.1002/2017WR020917.

916 Wing, O. E. J., Sampson, C. Bates, P. D., Quinn, N., Smith, A. M., Neal, J. C., C. (2019a).
917 A flood inundation forecast of Hurricane Harvey using a continental-scale 2D hydrodynamic
918 model. *Journal of Hydrology* X 4 , 100039.

919 Wing, O. E. J., Bates, P. D., Neal, J. C., Sampson, C. C., Smith, A. M., Quinn, N., et al.
920 (2019b). A New Automated Method for Improved Flood Defense Representation in Large-Scale
921 Hydraulic Models. *Water Resources Research* 55, 11007-11034, <https://doi.org/2019WR025957>

922 Yamazaki, D., Ikeshima, D., Tawatari, R., Yamaguchi, T., O'Loughlin, F., Neal, J.,
923 Sampson, C., Kanae, S., Bates, P. D. (2017). A high accuracy map of global terrain elevations.
924 *Geophysical Research Letters*.

925 Yamazaki, D., Ikeshima, D., Sosa, J., Bates, P. D., Allen, G. H., & Pavelsky, T. M. (2019).
926 MERIT Hydro: a high-resolution global hydrography map based on latest topography dataset.
927 *Water Resources Research*, 55, 5053–5073. <https://doi.org/10.1029/2019WR024873>

928 Zuzanna Zajac, Z., Zambrano-Bigiarini, M., Salamon, P., Burek, P., Gentile, A., Bianchi,
929 A., 2013. Calibration of the LISFLOOD hydrological model for Europe. JRC technical report
930 JRC87717.